J Biol Inorg Chem (2010) 15:689–700
DOI 10.1007/s00775-010-0636-z

ORIGINAL PAPER

Extended cardiolipin anchorage to cytochrome *c*: a model for protein–mitochondrial membrane binding

Federica Sinibaldi · Barry D. Howes · Maria Cristina Piro · Fabio Polticelli · Cecilia Bombelli · Tommaso Ferri · Massimo Coletta · Giulietta Smulevich · Roberto Santucci

Received: 23 November 2009 / Accepted: 14 February 2010 / Published online: 18 March 2010

Abstract Two models have been proposed to explain the interaction of cytochrome *c* with cardiolipin (CL) vesicles. In one case, an acyl chain of the phospholipid accommodates into a hydrophobic channel of the protein located close the Asn52 residue, whereas the alternative model considers the insertion of the acyl chain in the region of the Met80-containing loop. In an attempt to clarify which proposal offers a more appropriate explanation of cytochrome *c*–CL binding, we have undertaken a spectroscopic and kinetic study of the wild type and the Asn52Ile mutant of iso-1-cytochrome *c* from yeast to investigate the interaction of cytochrome *c* with CL vesicles, considered here a model for the CL-containing mitochondrial membrane. Replacement of Asn52, an invariant residue located in a small helix segment of the protein, may provide data useful to gain novel information on which region of cytochrome *c* is involved in the binding reaction with CL vesicles. In agreement with our recent results revealing that two distinct transitions take place in the cytochrome *c*–CL binding reaction, data obtained here support a model in which two (instead of one, as considered so far) adjacent acyl chains of the liposome are inserted, one at each of the hydrophobic sites, into the same cytochrome *c* molecule to form the cytochrome *c*–CL complex.

Keywords Cytochrome *c* · Site-directed mutagenesis · Cardiolipin · Mitochondrial membrane · Resonance Raman

F. Sinibaldi · M. C. Piro · M. Coletta · R. Santucci (✉)
Dipartimento di Medicina Sperimentale e Scienze Biochimiche,
Università di Roma "Tor Vergata",
Via Montpellier 1, 00133 Rome, Italy
e-mail: santucci@med.uniroma2.it

B. D. Howes · G. Smulevich
Dipartimento di Chimica,
Università degli Studi di Firenze,
50019 Sesto Fiorentino, FI, Italy

F. Polticelli
Dipartimento di Biologia,
Università Roma Tre,
00146 Rome, Italy

C. Bombelli
Istituto di Metodologie Chimiche del CNR,
c/o Dipartimento di Chimica,
Università di Roma "Sapienza",
00185 Rome, Italy

T. Ferri
Dipartimento di Chimica,
Università di Roma "Sapienza",
00185 Rome, Italy

Introduction

Cytochrome *c* is a peripheral membrane protein functioning in-between the inner and the outer membrane of the mitochondrion, mediating electron transfer between different proteins of the respiratory chain. It is a single-chain protein and possesses three major and two minor α-helices in the structure. The prosthetic group is covalently bound by two thioether bridges to two cysteine residues, Cys14 and Cys17. Under physiological conditions, His18 and Met80 are the axial ligands of the heme iron. Studies of engineered cytochrome *c* have significantly improved our knowledge of the role played by side chains (in particular, the invariant residues) in terms of structural stabilization, folding, and functionality [1–7]. In fact, yeast iso-1-cytochrome *c* is an ideal model system because its structure and properties in solution have been extensively studied [8–11],

and a system to produce mutants by site-directed mutagenesis has been developed [12, 13].

In the cellular environment a portion of cytochrome *c* is bound to cardiolipin (CL), one of the phospholipids constituting the mitochondrial membrane. Cytochrome *c* binding to CL produces a tertiary conformational rearrangement in the protein with formation of a nonnative but still compact structure characterized, as the molten globule [14, 15], by a perturbed heme crevice [16]. Similar behavior is observed in vitro when cytochrome *c* is mixed with CL liposomes under appropriate conditions; a stable (cytochrome *c*–CL) complex is formed at neutral pH and low ionic strength [17–21].

In addition to its electron transfer function carried out in the mitochondrion under normal conditions, cytochrome *c* plays a primary role in programmed cell death (cell apoptosis). In response to a variety of apoptosis-inducing agents, the protein is released into the cytosol where it actively participates in the execution of cell apoptosis by binding to the apoptosis protease activation factor, APAf-1, with subsequent activation of procaspase 9 [22, 23]. The peroxidase activity acquired by mitochondrial membrane-bound cytochrome *c* is critical during the early stages of the apoptotic process. The cytochrome *c*–CL complex acts as a powerful CL-specific peroxidase, generating CL hydroperoxides, which, having low affinity for the protein, favor complex dissociation and allow release of free soluble cytochrome *c* from the mitochondrial membrane into the cytosol [24]. Interestingly, on the basis of temperature-dependent conformational changes at pH 3.0 in the absence of lipids, it has recently been suggested that binding of CL to cytochrome *c* leads to a conformational switch to a β-sheet structure with the concomitant appearance of peroxidase activity and heme exposure [25]. Thus, whereas the native fold is important for cytochrome *c* to act as an electron carrier in mitochondria, the nonnative compact conformation of the CL-bound protein is essential for it to participate in the apoptotic program.

A better understanding of the mechanism(s) governing the cytochrome *c*–CL interaction is highly desirable. Determination of the structural properties of the cytochrome *c*–CL complex and of the factors affecting its stability is of importance since this would give more insight into how the early stages of the apoptotic process evolve. Previous work on the interaction of cytochrome *c* with CL liposomes revealed the presence in the protein of (at least) two protein binding sites, namely, the A-site and the C-site, characterized by different affinities for the phospholipid [17–20]. The interaction at the A-site was proposed to be of an electrostatic nature and involves positively charged residues of cytochrome *c* (possibly Lys72 and Lys73) and the deprotonated negatively charged phosphate group of the phospholipid. Conversely, at the C-site the protein interaction with CL liposome is hydrophobic and should be stabilized by hydrogen bonding between the Asn52 residue and the protonated phosphate group of the lipid.

According to the so-called extended lipid conformation hypothesis [18], at the C-site one acyl chain of the phospholipid accommodates into a hydrophobic channel of the protein which extends from the surface to the heme pocket region, whereas the other chain points in the opposite direction from the headgroup into the liposome. This hypothesis emphasizes greatly the role played by the Asn52 residue located at the C-site, since its interaction with the CL liposome is considered crucial for a correct insertion of the acyl chain into the protein. More recently, Kalanxhi and Wallace [21] reported that the insertion of the acyl chain may occur in the region of the Met80-containing loop, the acyl chain gaining entry into the protein in-between two parallel hydrophobic polypeptide stretches surrounded by positively charged residues (such as Lys72 and Arg91). These hypotheses identify two distinct regions of the macromolecule that may be involved in the interaction with CL vesicles. In an attempt to clarify this still widely debated point, we exploited the potential offered by site-directed mutagenesis to produce the Asn52Ile mutant from yeast iso-1-cytochrome *c*. Replacement of Asn52, an invariant residue located in a small helix segment of the protein (residues 49–54 in yeast

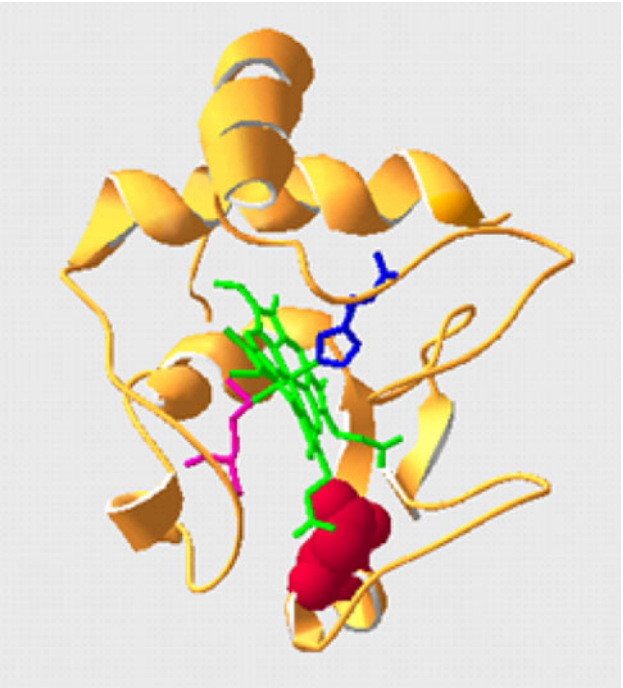

Fig. 1 Ribbon structure of yeast iso-1-cytochrome *c*. The heme group, with Fe(III) bound to His18 (*blue*) and Met80 (*magenta*), is represented in *green*. At the *bottom*, residue Asn52 is shown in *red*. The protein structure [8] was visualized with Swiss-Pdb

cytochrome *c*; see Fig. 1) is expected to provide new data useful to gain novel information on the role played by this residue in the cytochrome *c*–CL binding reaction. An earlier investigation reported that the Asn52Ile mutant displays higher stability than the wild-type protein [26]. Determination of whether Asn52 plays a primary role in the stabilization of the cytochrome *c*–CL complex is of importance because it would correlate Asn52 with the activation of the apoptotic process and provide additional evidence justifying the invariance of this residue in the sequence of *c*-class cytochromes.

Materials and methods

Materials

CL, as sodium salt from bovine heart (approximately 98% purity, lyophilized powder), was obtained from Sigma Chemical (St. Louis, MO, USA) and was used without further purification. All reagents used were of analytical grade.

Liposome preparation

Aqueous dispersions of CL liposomes were prepared according to a procedure described previously [27]. Briefly, a film of lipid was prepared on the inside wall of a round-bottomed flask by evaporation of a chloroform solution containing the proper amounts of lipid. The films obtained were stored in a dessicator overnight under reduced pressure and then 1 ml of a 20 mM *N*-(2-hydroxyethyl)piperazine-*N*′-ethanesulfonic acid buffer solution was added to obtain a 2.5 mM lipid dispersion. Solutions were vortex-mixed and then freeze–thawed six times from liquid nitrogen temperature to 30 °C. Dispersions were then extruded (ten times) through a 100-nm polycarbonate membrane. Extrusions were carried out at 30 °C.

Protein expression and purification

The expression plasmid pBTRI harboring both the yeast iso-1-cytochrome *c* gene (*CYC1*) and the heme lyase gene (*CYC3*) was a kind gift from A.G. Mauk of British Columbia University, Vancouver. The *CYC1* gene encodes the Cys102Thr variant of yeast iso-1-cytochrome *c*. In this variant, protein dimerization is precluded and the ferricytochrome autoreduction rate is greatly diminished. Since the optical and electrochemical properties are indistinguishable from those of iso-1-cytochrome *c* [12], the Cys102Thr variant is denoted here as "wild type."

Site-directed mutagenesis of the iso-1-cytochrome *c* gene (Cys102Thr variant) was performed directly on the pBTRI plasmid. Specific amino acid substitution (Asn52Ile) was introduced into yeast iso-1-cytochrome *c* using a QuikChange site-directed mutagenesis kit (Stratagene, La Jolla, CA) and the following oligonucleotides:

5′-TCGTACACAGATGCCATTATCAAGAAAAACG TGTTGTGG-3′

5′-CCACAACACGTTTTTCTTGATAATGGCATCTG TGTACGA-3′

Bacterial expression and purification of the recombinant protein were conducted essentially as previously described [14].

Escherichia coli strain JM 109 containing the pBTRI plasmid (or the mutated plasmid, see above) was grown at 37 °C, in 2 liters of superbroth medium containing 100 μg ml^{-1} ampicillin at an optical density of 0.3 at 600 nm. Induction was accomplished by adding isopropyl-*β*-D-thiogalactopyranoside to a final concentration of 0.75 mM. Cells were incubated at 37 °C overnight, harvested by centrifugation, and frozen at −80 °C. After they had thawed, the reddish pellets were resuspended in 50 mM tris(hydroxymethyl)aminomethane–HCl buffer, pH 8.0 (3–4 ml g^{-1} of wet cells). Lysozyme (1 mg ml^{-1}) and DNase (5 μg ml^{-1}) were added to the homogenized cells. The suspension was left in ice for 1 h and then sonicated for 1 min, at medium intensity, 50% duty cycle. After centrifugation for 30 min at 10,000*g* to remove cell debris, the clarified supernatant was dialyzed overnight versus 10 mM phosphate buffer, pH 6.2, and then loaded on a CM 52 column (40-ml bed volume) equilibrated with the same buffer. Purification was performed by washing the column with 1 vol of 45 mM phosphate buffer, pH 6.8, followed by 1 vol of 45 mM phosphate buffer + 75 mM NaCl, pH 6.8, and by successively eluting the protein with 1 vol of 45 mM phosphate buffer + 250 mM NaCl, pH 6.8. After purification, the recombinant Cys102Thr variant of yeast iso-1-cytochrome *c* and the Asn52Ile mutated protein (yield 5–7.5 mg l^{-1}) were promptly oxidized by adding a few grains of potassium ferricyanide and then subjected to extensive dialysis against 100 mM phosphate buffer, pH 7.0. The recombinant protein (approximately 50 μM) was more than 98% pure (from sodium dodecyl sulfate polyacrylamide gel electrophoresis analysis and reverse-phase high-performance liquid chromatography, data not shown) and stored at −80 °C in 200-μl aliquots.

Circular dichroism measurements

Circular dichroism (CD) measurements were carried out using a J-710 spectropolarimeter (JASCO, Tokyo, Japan) equipped with a PC as a data processor. The molar ellipticity ([θ]; deg cm^2 $dmol^{-1}$) is expressed on a molar heme basis in the Soret (400–450 nm) region. In the far-UV region, measurements (not shown) were carried out in the 215–250-nm range.

Binding of cytochrome *c* (as the wild type or the Asn52Ile variant) to CL liposomes was investigated by following the changes induced in the Soret CD spectrum (400–450 nm) of the protein by stepwise addition of a few microliters of a 2.5 mM CL buffered solution to a 10 μM (or 30) cytochrome *c* buffered solution ($V_i = 1.0$ ml; 0.5 cm pathlength cell). In both cases the buffer was 25 mM *N*-(2-hydroxyethyl)piperazine-*N*′-ethanesulfonic acid + 0.1 mM EDTA, pH 7.0. Dichroism spectra were recorded 10 min (wild type) or 25 min (Asn52Ile variant) after mixing.

Electronic absorption measurements

Electronic absorption measurements were carried out at 25 °C using a JASCO V-530 spectrophotometer and a double-beam Cary 5 spectrophotometer (Varian, Palo Alto, CA, USA). An extinction coefficient of $\varepsilon_{408} = 106\ \mathrm{mM}^{-1}\ \mathrm{cm}^{-1}$ was used to determine the concentration of wild-type and mutated cytochrome *c*.

Fast kinetics measurements

Kinetic measurements were carried out employing a rapid-mixing stopped-flow apparatus (SX.18 MV, Applied Photophysics, Salisbury, UK) with 1-ms dead time, equipped with a diode array for transient spectra collection over the 350–700-nm wavelength range.

Ferric cytochrome *c* was mixed with CL and absorption transient spectra were collected with a 1-ms time resolution between 350 and 700 nm. Further analysis was then carried out on progress curves at 695 nm, with a 1 cm pathlength cell.

Kinetic progress curves were fitted according to the following equation:

$$A_{\mathrm{obs}} = A_{\infty} \pm \sum_{i=1}^{i=n} \Delta A_i \exp^{\left(-(k_i t)^{\beta}\right)}, \qquad (1)$$

where A_{obs} is the absorption at 695 nm at a given time interval, A_{∞} is the final absorption (when the reaction is complete), ΔA_i is the signal change for phase *i*, k_i is the rate constant for phase *i*, *t* is time, and β is a phenomenological factor, referable to the cooperativity of the kinetic process ($\beta > 1$ for positive cooperativity, $\beta < 1$ for negative cooperativity, and $\beta = 1.0$ for no cooperativity). The sign $\pm$ indicates that, depending on the wavelength, the signal may either decrease or increase.

Resonance Raman measurements

Resonance Raman spectra were obtained using a 5-mm NMR tube and by excitation with the 406.7-nm line of a Kr^+ laser (Innova 300 C, Coherent, Santa Clara, CA, USA). Backscattered light from a slowly rotating NMR tube was collected and focused into a triple spectrometer (consisting of two Acton Research SpectraPro 2300i and a SpectraPro 2500i in the final stage with a 3,600 grooves per millimeter grating) working in the subtractive mode, equipped with a liquid-nitrogen-cooled CCD detector. It should be noted that the spectral resolution of the resonance Raman spectra cited in the figure captions is that calculated theoretically on the basis of the optical properties of the spectrometer. However, for the moderately broad experimental resonance Raman bands observed in the present study (about 10 cm^{-1}), the effective spectral resolution will in general be lower. The resonance Raman spectra were calibrated with indene and CCl_4 as standards to an accuracy of 1 cm^{-1} for intense isolated bands. The spectral changes induced by CL liposomes were monitored following the stepwise addition of 2-μl aliquots of CL (3 mM) buffered solution to 150 μl of a 30 μM protein buffered solution, recording the spectrum 30 min after mixing.

Results

Structural properties of the Asn52Ile mutant

CD measurements

The Asn52Ile mutant shows a well-defined far-UV dichroism spectrum typical of proteins with α-helix secondary structure (not shown); the ellipticity at 207 and 221 nm is approximately 10% higher than that of the wild-type form. Figure 2 shows the Soret CD spectrum

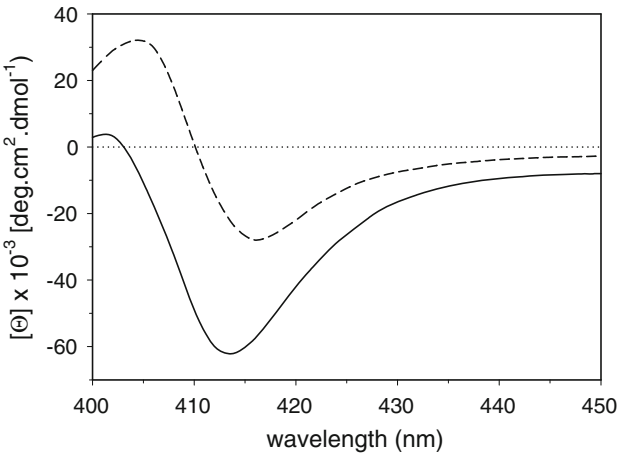

Fig. 2 Soret circular dichroism (CD) spectrum of the Asn52Ile mutant (*solid line*). The CD spectrum of the wild-type protein (*dotted line*) is reported for comparative purposes. The experimental conditions were 100 mM phosphate buffer, pH 7.0, and 25 °C

(400–450 nm, strictly correlated with the heme pocket structure), in which the Cotton effect centered at 416 nm for the wild-type protein is blueshifted (by approximately 2 nm) and markedly stronger in the mutant. This signal has been attributed to the Phe82–heme and Met80–heme interaction and is considered a probe of the environment on the Met80 side of the heme pocket [28, 29].

Stability of the Asn52Ile mutant

The stability of the Asn52Ile mutant was investigated by CD at 222 nm, following protein unfolding induced by guanidine hydrochloride (spectra not shown). The process is reversible and reaches completion in a few minutes. The thermodynamic parameters of the transitions, reported in Table 1, indicate that the Asn52Ile variant shows an increased stability with respect to the wild-type protein. The ΔG_0 value, i.e., the apparent free-energy change in the absence of denaturant, was estimated by extrapolating the curve to zero denaturant concentration on the assumption of a linear dependence of the apparent free-energy change (ΔG_D) versus denaturant concentration [30]. The value of ΔG_D was obtained from the apparent denaturation equilibrium constant, K_D, determined by the expression $K_D = (\theta_i - \theta_{obs})/(\theta_{obs} - \theta_f)$, where θ_i, θ_f, and θ_{obs} represent the initial, final, and observed values of the ellipticity, respectively. The thermodynamic parameters for the unfolding titration (see Table 1) provide quantitative indication for the markedly higher stability of the Asn52Ile mutant with respect to the wild-type protein ($\Delta G_0 = 47.3 \pm 1.1$ vs. 22.4 ± 1.1 kJ mol^{-1}). The data also suggest that the variant has a compactness comparable to that of the wild-type protein, as indicated by the values of m (12.5 vs. 12.4 kJ mol^{-1} M^{-1}), a parameter that directly measures the dependence of ΔG_D on the denaturant concentration according to the empirical equation $\Delta G_D = \Delta G_0 - m[D]$, where [D] is the denaturant concentration. m is assumed to be proportional to the change of accessible area of a protein upon unfolding [30, 31].

Table 1 Denaturation parameters of the N52I mutant of iso-1-cytochrome *c*

	$C_{1/2}$[a] (M)	ΔG_0 (kJ mol^{-1})	m (kJ mol^{-1} M^{-1})
Wild-type cytochrome *c*	1.8	22.4	12.4
N52I mutant	2.4	47.3	12.5
Horse cytochrome *c*[b]	2.5	33.5	13.4

The experimental conditions were 0.1 M phosphate buffer, pH 7.0, and 25 °C. Thermodynamic parameters are determined from circular dichroism studies in the helix region (see the text for details). The estimated errors in $C_{1/2}$, ΔG_0, and m are ±0.1 M, ±1.1 kJ M^{-1}, and ±0.9 kJ mol^{-1} M^{-1}, respectively

[a] Denaturant concentration at the midtransition point

[b] From [15]

The Asn52Ile mutant–CL liposome interaction

Previous studies on equine ferricytochrome *c* have shown that formation of the CL–cytochrome *c* complex is associated with changes of the tertiary structure of the protein, with a marked alteration of the heme pocket region, and with the displacement of Met80 from the sixth coordination position of the heme iron [18–21]. In this paper we extend the investigation to yeast iso-1-ferricytochrome *c* as, in contrast to horse cytochrome *c*, a stable Asn52Ile mutant of the protein from yeast is obtained by site-directed mutagenesis. Figure 3 shows the Soret CD spectrum of the mutant recorded at neutral pH in the absence and in the presence of large (approximately 100 μm) CL unilamellar liposomes. The dramatic decrease of the 414-nm Cotton effect induced by CL indicates that cytochrome *c* binds to CL vesicles (the CL concentration used was higher than its critical micelle concentration) and that such interaction alters the heme pocket region. However, unlike the wild-type protein (whose spectrum is shown in the inset in Fig. 3), a weak dichroic signal still remains visible, suggesting that part of the mutated protein population maintains the Fe(III)–Met80 bond unaltered. It is underlined that for our experimental conditions, free cytochrome *c* is characterized by a well-defined negative 416-nm Cotton effect. The disappearance of such a negative band upon addition of CL liposomes to the protein solution (6:1 molar

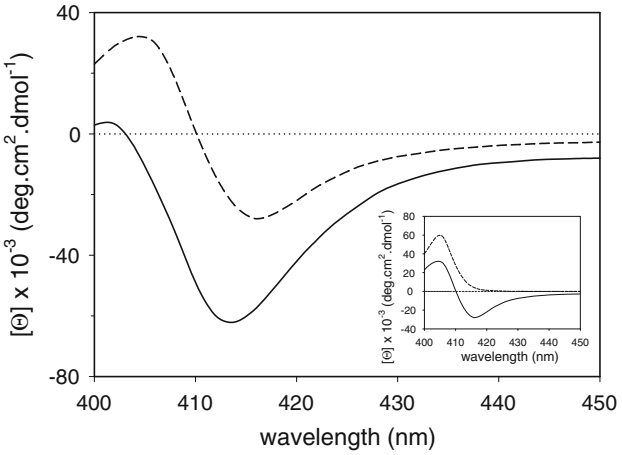

Fig. 3 Cardiolipin (CL) vesicles binding to the Asn52Ile mutant. Soret CD spectrum of mutated cytochrome *c* obtained in the absence (*solid line*) and in the presence (*dotted line*) of CL (6:1 CL to cytochrome *c* molar ratio). The experimental conditions were 10 μM protein, 20 mM *N*-(2-hydroxyethyl)piperazine-*N*′-ethanesulfonic acid (Hepes) + 0.1 mM EDTA, pH 7.0, and 25 °C. The *inset* shows the same measurements carried out on the wild-type protein under the same experimental conditions

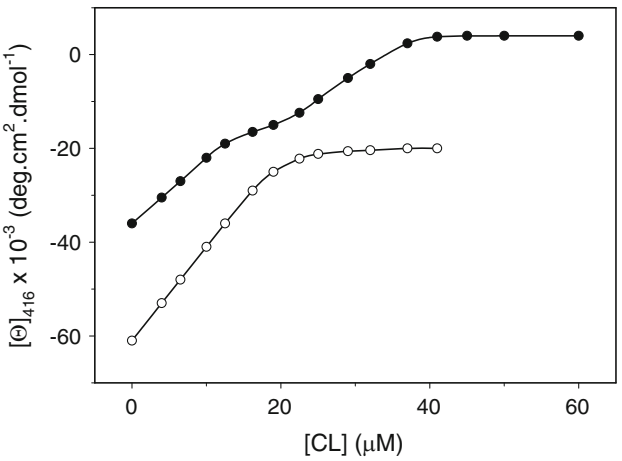

Fig. 4 Titration curve of CL vesicles binding to the Asn52Ile mutant (*open circles*) and to wild-type yeast iso-1-cytochrome *c* (*filled circles*) showing the variation of the 416-nm (414 nm for the mutant) Cotton effect induced by stepwise addition of CL to a 10 μM cytochrome *c* solution. Experimental points are the average of at least three measurements. Other conditions are as for Fig. 3

ratio) reveals that all the protein is fully bound to the lipid. The binding reaction with CL vesicles is characterized by a slow equilibrium (as illustrated in the inset in Fig. 5). Approximately 97% of the mutant is bound to CL in 18–20 min after mixing, whereas approximately 100% of the wild-type protein is CL-bound after 3–4 min. As already observed for the equine protein [24], the stepwise addition of CL liposomes to a wild-type cytochrome *c* solution gives rise to two distinct transitions during complex formation (Fig. 4). Conversely, the binding of the Asn52Ile mutant (also illustrated in Fig. 4) is characterized by a two-state transition, suggesting that in this case only one site of the protein interacts with CL vesicles. When reacting with CL, yeast iso-1-cytochrome *c* and the Asn52Ile variant form very stable complexes which do not dissociate in the presence of 0.5 M NaCl, unlike that observed for the equine cytochrome *c* [24].

Stopped-flow kinetics

Figure 5 shows the CL-binding kinetics of wild-type cytochrome *c* and the Asn52Ile mutant, monitored by following the absorbance at 695 nm (which is strictly correlated to the Fe(III)–Met80 axial bond [32]). According to Eq. 1, the analysis of kinetic progress curves requires two exponentials ($n = 2$ in Eq. 1) both for the wild-type protein and for the Asn52Ile mutant. The data indicate that the CL-binding kinetics of the wild-type protein is characterized by a main fast event having a rate constant, $k_1 = 0.36\ s^{-1}$ (±0.05), which is about sixfold lower than that determined for horse cytochrome *c* [20]. This reflects the existence of a higher energy barrier for the interaction with CL vesicles. The main process is then followed by a minor event at slightly slower rate [i.e., $k_2 = 0.071\ s^{-1}$ (±0.009)]. As previously observed for the equine protein [20], the rate constant of the binding reaction is independent of CL concentration (data not shown), suggesting the existence, also in this case, of a rate-limiting step perhaps represented by the Fe(III)–Met80 bond cleavage.

In agreement with the CD data (shown in the inset in Fig. 5), the Asn52Ile-CL interaction kinetics is significantly slower than that of the wild-type protein and is characterized by a cooperative behavior. The data show that a large absorbance change with rate constant $k_2 = 2.6 \times 10^{-3}\ s^{-1}$ (±0.4) (thus, about 100-fold lower than that determined for the wild-type protein) follows a minor faster event [$k_1 = 7.0 \times 10^{-3}\ s^{-1}$ (±1.0)]. Thus, compared with wild-type cytochrome *c*, a higher energy barrier [approximately 12 kJ mol^{-1}, most of which is necessary for the cleavage of the Fe(III)–M80 bond] is encountered by the acyl chain of the phospholipid upon binding to the mutant.

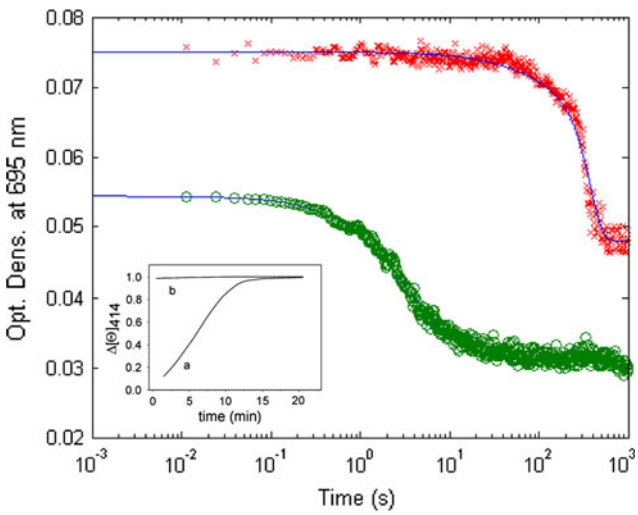

Fig. 5 Kinetics of CL vesicles binding to wild-type cytochrome *c* (*circles*) and to the Asn52Ile mutant (*crosses*), monitored by following the absorbance at 695 nm. The kinetic progress curves have been shifted for the sake of clarity and they were recorded after mixing a CL (150 μM final concentration) solution with the protein (wild type or mutant) solution (30 μM final concentration). *Continuous lines* represent the nonlinear least-squares fitting of data according to Eq. 1, employing two exponentials. In the case of wild-type cytochrome *c*, the parameters are $OD_\infty = 0.031 \pm 0.005$, $\Delta OD_1 = 0.017 \pm 0.003$, $k_1 = 0.36\ s^{-1}$ (±0.05), $\Delta OD_2 = 0.007 \pm 0.001$, $k_2 = 0.071\ s^{-1}$ (±0.009) (where OD is optical density), with $\beta = 1.0$ for both processes. In the case of the Asn52Ile mutants, the parameters are $OD_\infty = 0.048 \pm 0.007$, $\Delta OD_1 = 0.008 \pm 0.001$, $k_1 = 7.0 \times 10^{-3}\ s^{-1}$ (±1.0), $\Delta OD_2 = 0.019 \pm 0.003$, $k_2 = 2.6 \times 10^{-3}\ s^{-1}$(±0.4), with $\beta = 1.0$ for process 1 and $\beta = 3.3$ for process 2. The *inset* shows the kinetic progress curves of the Asn52Ile mutant (*line a*) and of wild-type cytochrome *c* (*line b*) recorded by CD at 414 and 416 nm, respectively, after addition of 60 μM CL vesicles to a 10 μM protein solution (other conditions are as for Fig. 3)

Resonance Raman measurements

Figures 6 and 7 show the effects of the stepwise addition of CL liposomes on the electronic absorption and resonance Raman spectra of the ferric wild-type and Asn52Ile mutant proteins at pH 7.0, respectively. The spectra of the wild-type and mutant proteins at alkaline pH in the absence of CL are also shown for comparison. The UV–vis spectra of the wild-type protein display only slight variations upon increasing the CL to protein molar ratio, except for a clear increase in scattering due to the liposomes, which is the probable origin of the blueshift of the Q_1 band at 530 nm. Conversely, the resonance Raman spectra are very sensitive to the presence of CL. The high-frequency resonance Raman spectra (Fig. 6c) display a progressive upshift of the bands upon addition of CL in the CL to cytochrome *c* ratio interval between 3 and 5, after which no further variations are observed. The pronounced saddling distortion of the wild-type protein [33] is reflected in the resonance Raman spectrum by lower core size marker band frequencies compared with planar heme proteins, which display an inverse correlation between resonance Raman band frequencies and the porphyrin core size [34–36]. Hence, interaction of CL with cytochrome *c* gives rise to a less distorted heme. Interestingly, the ν_{11} resonance Raman band upshifts from 1,561 cm^{-1} (CL to cytochrome *c* molar ratio of 0) to 1,564 cm^{-1} at higher CL to cytochrome *c* molar ratios. An analogous effect has been observed for the alkaline form of cytochrome *c* (Fig. 6c), characterized by Lys–Fe–His coordination [37], and the yeast His26Tyr mutant, characterized by a substantial subpopulation with Lys–Fe–His coordination [14]. This observation suggests the growth of a misligated Lys–Fe–His species when cytochrome *c* binds to CL vesicles. The most significant variations upon addition of CL to note in the low-frequency spectra (Fig. 6b) are (1) the increase in the relative intensity of the band at 413 cm^{-1}, (2) intensification of the band at 693 cm^{-1} compared with that at 702 cm^{-1}, and (3) reduced intensity of the weak out-of-plane modes in the interval from 440 to 670 cm^{-1} (particularly γ_{21} at 568 cm^{-1}). These changes are largely complete by a CL to cytochrome *c* molar ratio of 3. At molar ratios greater than 5 no further variations are observed (in agreement with data on horse cytochrome *c* [20]). Similar spectral variations have been observed previously in the low- and high-frequency resonance Raman spectra of cytochrome *c* following a change in axial coordination, in which a misligated Lys or His residue replaces the native Met80 residue, leading to a relaxation of the heme distortion [14, 15, 38–43]. In particular, it has been reported that the low-frequency resonance Raman bands in the 340–420-cm^{-1} region can provide a means to

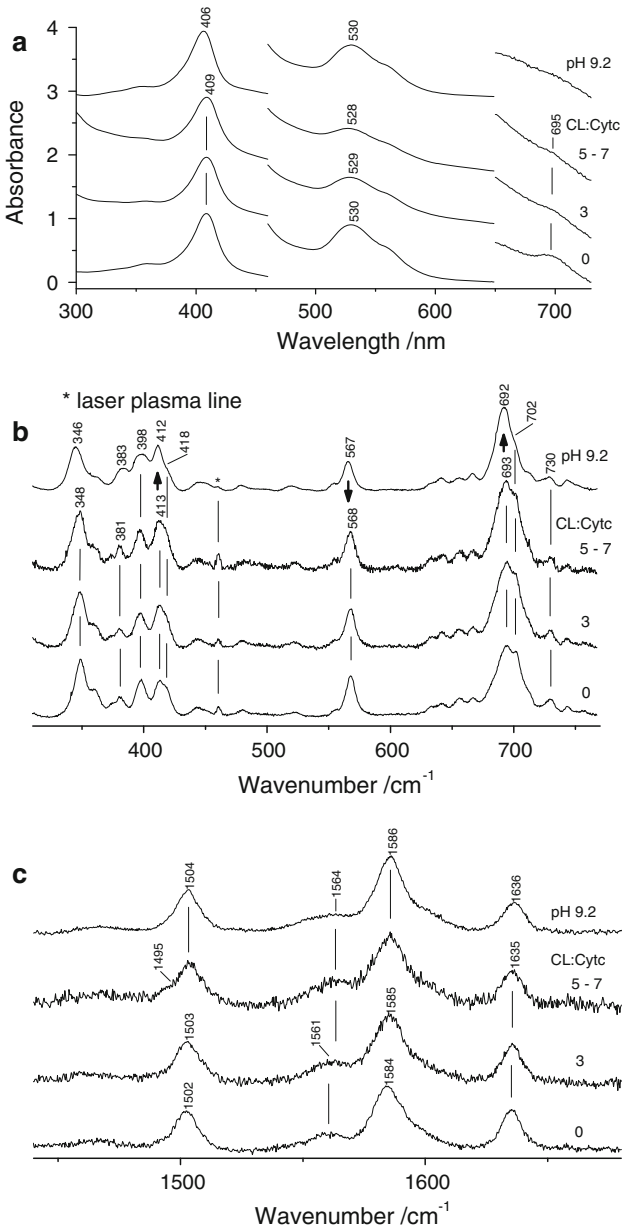

Fig. 6 Electronic absorption and resonance Raman spectra of 30 μM wild-type cytochrome *c* in 20 mM Hepes + 0.1 mM EDTA, pH 7.0, for increasing concentrations of CL vesicles. The CL to cytochrome *c* molar ratio is shown for each spectrum. In the molar ratio interval 5–7 no spectral variations are observed. The spectra of the wild-type protein at pH 9.2 in 50 mM glycine are also shown for comparison. The 460–650- and 650–730-nm regions of the absorption spectra (**a**) are expanded 8- and 100-fold, respectively. The ordinate scale refers to the protein at pH 7.0 in the absence of CL. The experimental conditions for the high-frequency (**c**) and low-frequency (**b**) resonance Raman spectra were excitation wavelength 406.7 nm, spectral resolution 1 cm^{-1}, laser power at the sample 10 mW, and integration time 10 min. The intensities are normalized to that of the ν_4 band (not shown). The *asterisk* indicates a laser plasma line. The *arrows* in the low-frequency resonance Raman spectra indicate the variations in band intensities which follow interaction of the protein with CL

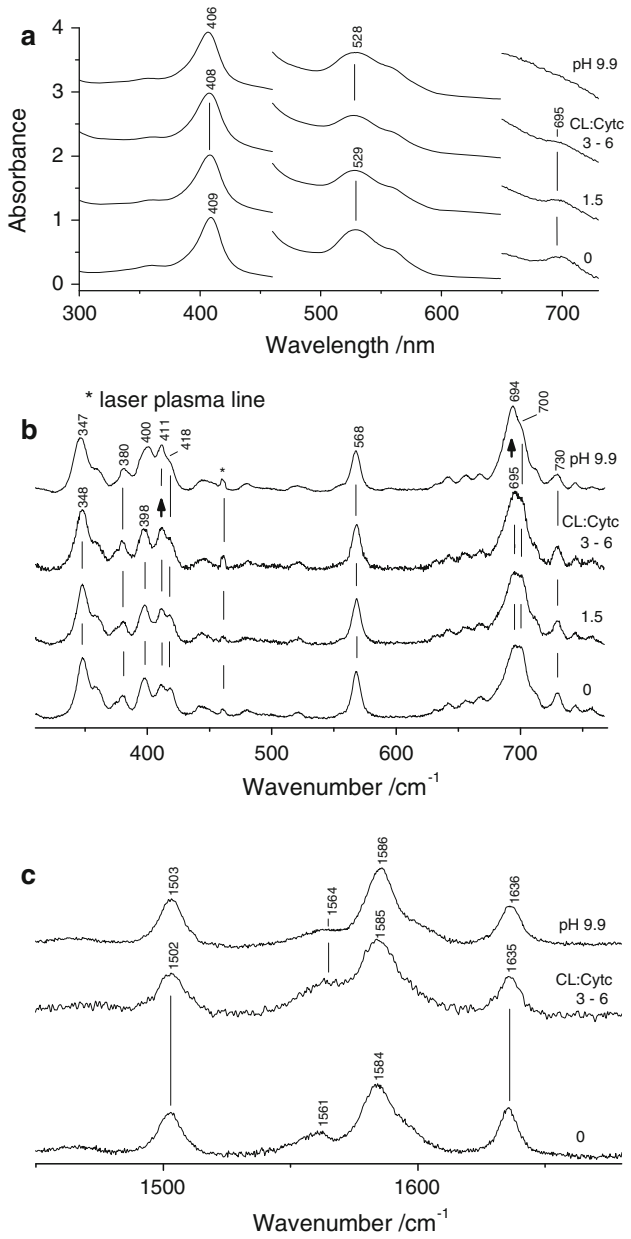

Fig. 7 Electronic absorption and resonance Raman spectra of 30 μM Asn52Ile mutant in 20 mM Hepes + 0.1 mM EDTA, pH 7.0, for increasing concentrations of CL. The CL to cytochrome *c* molar ratio is shown for each spectrum. In the molar ratio interval 3–6 no spectral variations are observed. The spectra of the mutant protein at pH 9.9 in 50 mM glycine are also shown for comparison. The 460–650- and 650–730-nm regions of the absorption spectra (**a**) are expanded 8- and 100-fold, respectively. The ordinate scale refers to the protein at pH 7.0 in the absence of CL. The experimental conditions for the high-frequency (**c**) and low-frequency (**b**) resonance Raman spectra were excitation wavelength 406.7 nm, spectral resolution 1 cm^{-1}, laser power at the sample 10 mW, and integration time 10 min. The intensities are normalized to that of the ν_4 band (not shown). The *asterisk* indicates a laser plasma line. The *arrows* in the low-frequency resonance Raman spectra indicate the variations in band intensities which follow interaction of the protein with CL

distinguish between hexacoordinate low-spin species in which the sixth ligand is Lys or His [42]. The changes observed for the 413 and 418 cm^{-1} bands upon addition of CL are very similar to those found upon mutation of cytochrome *c* His26 [14], binding of oleic acid to cytochrome *c* [43], or following the alkaline transition of cytochrome *c* (Fig. 6b), in which the Met80 axial ligand is replaced by Lys73 and Lys79 [37]. They are not consistent with the changes observed when cytochrome *c* adopts a bis-His coordination [44], where a significant intensity increase is expected at 418 cm^{-1}. Hence, the changes noted upon interaction of cytochrome *c* with CL are consistent with the growth of a misligated species in which the heme is characterized by a Lys–Fe(III)–His coordination. At CL to protein molar ratios in the interval from 5 to 7, the ν_3 resonance Raman band due to a pentacoordinate high-spin species appears at 1,495 cm^{-1}. Similar effects have been reported previously upon cytochrome *c* binding to dioleoylphosphatidylglycerol phospholipid liposomes [45].

The electronic absorption and resonance Raman spectra of the Asn52Ile mutant in the absence of CL are very similar to those of the wild-type protein. The most evident variation regards a slight intensification of the out-of-plane γ_5 mode (730 cm^{-1}) compared with the wild-type protein (Fig. 7b). In agreement with the CD measurements, the variations in the UV–vis (Fig. 7a) and resonance Raman (Fig. 7b, c) spectra induced by CL binding in the case of the Asn52Ile mutant are observed up to a CL to protein molar ratio of 3, after which no further changes are noted. The spectral modifications (reduction of the 695 nm band intensity, an upshift of the ν_{11} and ν_2 resonance Raman bands at 1,561 and 1,584 cm^{-1}, respectively, and a progressive slight intensification of the bands at 411 and 695 cm^{-1}) are the same as those evident for the wild-type protein upon interaction with CL, but are less pronounced. Furthermore, as noted for the wild-type protein, similar spectral variations are observed for the alkaline form of the mutant. By analogy with the wild-type alkaline form, a Lys residue is assumed to replace the axial Met80 residue in the alkaline form of the mutant. In fact, very similar spectral modifications are observed for both proteins at alkaline pH (Figs. 6, 7). It is worthy of note that the 695 nm band in the UV–vis spectrum of the mutant, characteristic of Met–His axial coordination, is not completely bleached until pH 9.9, indicating that the pK_a of the mutant alkaline transition is higher than that of the wild-type protein. A similar effect has been reported for a number of other cytochrome *c* mutants [37]. Therefore, it is apparent that only a relatively small population of a misligated low-spin species with Lys-His coordination is formed upon CL binding to the mutant. This result is consistent with the kinetic data reported in

Fig. 5, which reveal that CL has a relatively minor effect on the mutant compared with the wild-type protein. Hence, either the Asn52Ile mutant has a relatively weak interaction with CL, which can be excluded as the mutant has high affinity for CL (Fig. 4), or the interaction with CL leads to more limited structural variations of the heme pocket.

Discussion

CL represents approximately 25% of the total amount of lipids forming the mitochondrial membrane [46]. About 15% of mitochondrial cytochrome *c* is tightly bound to the phospholipid, whereas the remainder is free or loosely bound via electrostatic interactions and can be readily mobilized. The loosely bound cytochrome *c* participates in electron transfer, inhibits reactive oxygen species formation, and prevents oxidative stress, whereas the tightly bound cytochrome *c* does not participate in electron transfer but it is thought to give rise to peroxidase activity, an event crucial for initiating the apoptotic process. It is known that during apoptosis cytochrome *c* is released from the mitochondrial interface space into the cytosol, which implies protein dissociation from the mitochondrial membrane. This reveals that the cytochrome *c*–CL interaction plays an important role in the cell, modulating the protein behavior and determining whether cytochrome *c* must carry out its "normal" role in the respiratory chain within the intermembrane space, or is to be released into the cytosol and participate in the apoptotic event.

In this study we have investigated the interaction of cytochrome *c* with CL vesicles, considered here a model for the CL-containing mitochondrial membrane. As has been demonstrated over the last 15–18 years, cytochrome *c* avidly interacts with CL-containing liposomes, forming a stable cytochrome *c*–CL complex. Thus, specifically, the interaction of cytochrome *c* with CL liposomes was reported herein. Previous work suggests that binding of CL liposomes to cytochrome *c* occurs at two distinct sites of the protein (namely, the A-site and the C-site) having different affinities for the phospholipid [20]. The region comprising the Asn52 residue is thought to be critical in cytochrome *c* binding to CL [18]; hydrogen bonding between Asn52 and the protonated phosphate group of the CL liposome is expected to promote the acyl chain insertion into the protein through a hydrophobic channel close to residue 52. In wild-type cytochrome *c* Asn52 forms a short helix segment with three other side chains located in a highly hydrophobic environment. The increased stability of the Asn52Ile mutant (Table 1) with respect to the wild-type protein may be in part due to the substitution of a helix-breaking residue (Asn) with a helix-forming residue (Ile). However, other factors seem to contribute to mutant stabilization, such as the enhanced hydrophobicity of the loosely packed region around the heme propionates (induced by Ile52) [26] and the interaction of Ile52 with nearby hydrophobic residues. The latter effect, which plays a major role in the overall structure stabilization, is likely responsible for the slower kinetics of the acyl chain insertion into cytochrome *c*, which depends, at least in part, on the relative movement of the 50's helix with respect to the 75–87 loop (i.e., the Met80-containing segment). Thus, the residue located at position 52 is significantly involved in complex formation. The slower binding kinetics depends on several factors. First, the mutation-induced stabilization of the (51–54 residues) helix, which, hindering the chain penetration into the hydrophobic channel, leads to a higher energy barrier for helix distortion (or unfolding). Another major factor is the distortion of the hydrophobic channel following the Asn52Ile mutation. In wild-type cytochrome *c* this channel, which has the correct shape and length to host the CL acyl chain, has a number of hydrophobic residues (Ile35, Trp59, Met64, Tyr67, and Ile75) close to Asn52, forming a loosely packed region around the heme propionates and able to host the acyl chain without significant structural rearrangements (see below). The distortion of the hydrophobic channel in the mutant leads to a rearrangement that significantly influences the structural and functional properties of the protein. One of the two binding sites is hindered (Fig. 4) and the other becomes less accessible to the chain insertion (Fig. 5). Several pieces of spectroscopic evidence support the view that the Asn52Ile mutation induces distortion of the hydrophobic channel: the observed modification of the 416-nm Cotton effect (Fig. 2), the relatively minor CL-induced variations of the resonance Raman and UV–vis spectra (when compared with the wild-type protein; Fig. 6), and the significantly slower binding kinetics shown by the mutated protein (Fig. 5).

An alternative to the cytochrome *c*–CL binding model introduced by Rytömaa and Kinnunen [18] is the proposal by Kalanxhi and Wallace [21] in which binding of CL vesicles to the protein is supposed to occur in the region of the Met80-containing loop. In this case, the acyl chain is assumed to penetrate into the protein between hydrophobic strands 67–71 and 82–85 and the phospholipid anchors to the protein via electrostatic interactions involving the deprotonated phosphate group of the CL liposome and the Lys72 residue of cytochrome *c*. The electrostatic and hydrophobic interactions control different aspects of cytochrome *c* binding to CL. The former govern the initial protein–CL molecular recognition, whereas the latter play a major role in cytochrome *c*–CL complex stabilization, since they allow insertion of the acyl chain into the protein. Both regions considered by these models have the potential to provide suitable sites for CL binding. In particular, as

Table 2 The hydrophobic patches of cytochrome *c* proposed to interact with the acyl chain of cardiolipin

	Residues								
	43	44	45	46	81	82	83	84	85
Horse cytochrome *c*	Ala	Pro	Gly	Phe	Ile	Phe	Ala	Gly	Ile
Yeast iso-1-cytochrome *c*	Ala	Glu	Gly	Tyr	Ala	Phe	Ala	Gly	Leu

reported in Table 2, the hydrophobic patches of the two sites can interact with an acyl chain of CL. Furthermore, when CL was manually docked onto the cytochrome *c* structure, we found that the acyl chain could be easily accommodated both in the hydrophobic channel in the vicinity of Asn52 (Fig. 8a) and in the region of the Met80-containing loop (Fig. 8b). In fact, in the latter case, the analysis demonstrated that CL can interact with the highly hydrophobic patch constituted by residues Tyr67, Leu68,

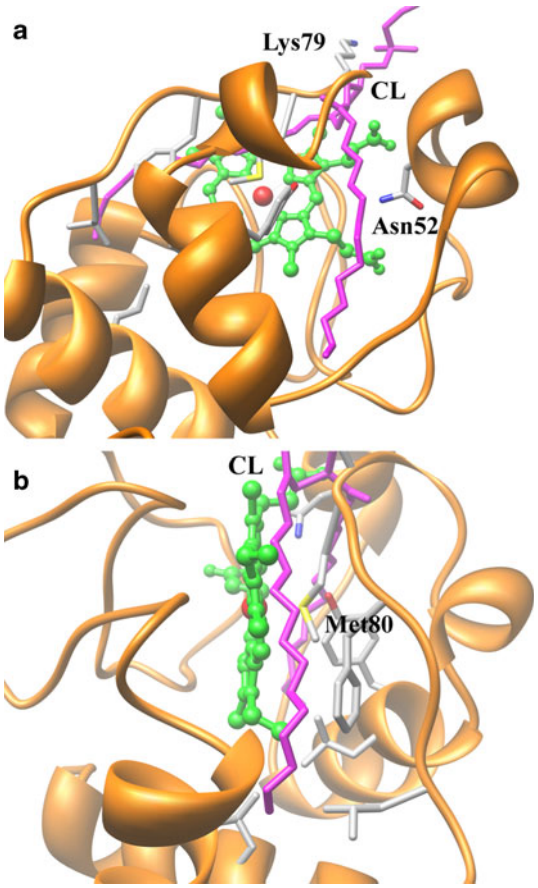

Fig. 8 The CL acyl chain putative binding sites within cytochrome *c*. **a** Insertion of a CL acyl chain into the hydrophobic pocket surrounding Asn52. **b** Insertion of a CL acyl chain into the hydrophobic pocket surrounding Met80. The CL moiety is shown in *magenta*, heme is shown in *green*, and the iron ion is shown as a *red sphere*. Note the putative interaction between Lys79 and one of the CL phosphate groups

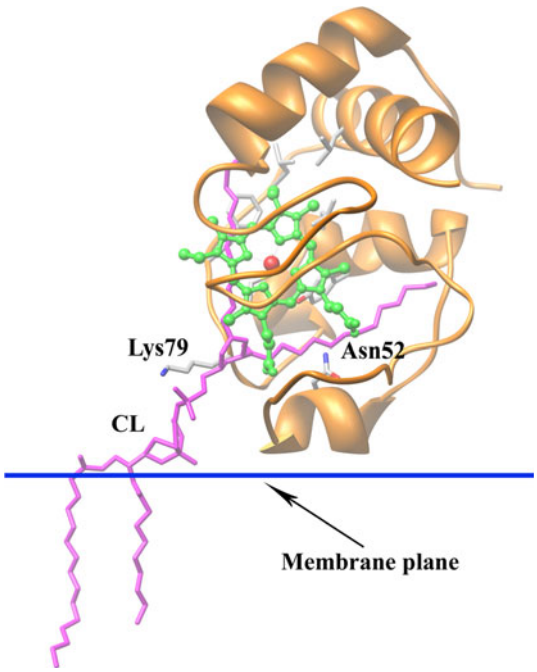

Fig. 9 A putative 1:1 complex of CL with cytochrome *c* showing the acyl chain binding sites within cytochrome *c*. Note the stereochemical compatibility of insertion of two acyl chains of CL into the two hydrophobic pockets illustrated in Fig. 8, with the concomitant insertion of the other two CL acyl chains within the mitochondrial membrane plane

Phe82, Leu85, and Leu94 and the deprotonated phosphate group of CL liposome can interact electrostatically with the Lys72 and Lys73 residues. A study of the adduct formed by carbon monoxide with the cytochrome *c*–CL complex [47] has also provided evidence in support of the Kalanxhi and Wallace proposal. This investigation revealed that the cytochrome *c*–CL-CO complex is stabilized by five to six positive charges on the surface of the protein, consistent with binding of CL in a region of positively charged residues.

Thus, at present the mode by which the protein interacts with CL vesicles is still unclear. The two-transition CL–cytochrome *c* binding process observed in this (and in a previous [20]) investigation suggests an alternative interaction mechanism in which two (instead of one, as considered to date) adjacent acyl chains of the CL liposome protrude, one at each of the hydrophobic sites, into the same cytochrome *c* molecule to form the cytochrome *c*–CL complex. In this model, illustrated in Fig. 9, we assume that upon binding of the first acyl chain at the high-affinity site, the tertiary structural rearrangement occurring in cytochrome *c* favors the insertion of a second acyl chain at the level of the low-affinity site. The view that two acyl chains bind to the protein at distinct times is in agreement with the observed two-transition binding process (Fig. 4) and with the biphasic character of the binding kinetics

(Fig. 5). This hypothesis is also very realistic from a stereochemical viewpoint, in that insertion of only one acyl chain into cytochrome *c* would cause partial exposure to the solvent of (at least) one of the adjacent acyl chains in the liposome, a situation disfavored from a solvation energy viewpoint.

The present results identify a Lys as the residue which most likely replaces Met80 at the sixth coordination position of the heme iron upon complex formation (Figs. 6, 7). Although the experimental data do not allow an unequivocal identification of the residue substituting Met80 as the axial ligand of the heme iron, Lys79 may be reasonably considered as the likely candidate, since Lys72 and Lys73 are involved in the electrostatic interaction with a deprotonated phosphate group of the CL liposome. In a previous study in which micelles were used as a membrane model, a low-spin state formed upon association of cytochrome *c* with the micelles and characterized by different spectral characteristics with respect to wild-type cytochrome *c* was also suggested to result from Lys79 binding to the heme [48]. Furthermore, the resonance Raman and CD spectra are very similar to those reported herein. The authors considered improbable the binding of a His residue, which has been suggested by some data in the literature [49–51], as similar results were obtained when the potential His ligands had been carbethoxylated.

In conclusion, the data presently available indicate that the cytochrome *c*–CL binding reaction is a complex, difficult to define event. However, in good accord with the large body of data reported in recent years, the model proposed here in which two adjacent acyl chains of the CL liposome protrude into the same cytochrome *c* molecule to form the cytochrome *c*–CL complex provides a significant contribution to better define the mechanism(s) leading to the cytochrome *c*–CL complex formation.

Acknowledgments This research was funded in part by grants from the Italian MIUR (PRIN 2007KAWXCL to R.S. and FIRB RBNE03PX83 to M.C.) and local Italian Grant (ex 60%) to G.S.

References

1. Rafferty SP, Pearce LL, Barker PD, Guillemette JG, Kay CM, Smith M, Mauk AG (1990) Biochemistry 29:9365–9369
2. Berghuis AM, Guillemette JG, Smith M, Brayer GD (1994) J Mol Biol 235:1326–1341
3. Lo TP, Guillemette JG, Louie GV, Smith M, Brayer GD (1995) Biochemistry 34:163–171
4. Lo TP, Komar-Panicucci S, Sherman F, McLendon G, Brayer GD (1995) Biochemistry 34:5259–5268
5. Marmorino JL, Pielak GJ (1995) Biochemistry 34:3140–3143
6. Rafferty SP, Guillemette JG, Berghuis AM, Smith M, Brayer GD, Mauk AG (1996) Biochemistry 35:10784–10792
7. Doyle DF, Waldner JC, Parikh S, Alcazar-Roman L, Pielak GJ (1996) Biochemistry 35:7403–7411
8. Louie GV, Brayer GD (1990) J Mol Biol 214:527–555
9. Baistrocchi P, Banci L, Bertini I, Turano P, Bren KL, Gray HB (1996) Biochemistry 35:13788–13796
10. Hildebrandt P (1996) In: Scott RA, Mauk AG (eds) Cytochrome *c*. A multidisciplinary approach. University Science Books, Sausalito, pp 285–314
11. Banci L, Bertini I, Bren KL, Gray HB, Sompornpisut P, Turano P (1997) Biochemistry 36:8992–9001
12. Cutler RL, Pielak GJ, Mauk AG, Smith M (1987) Protein Eng 1:95–99
13. Pollock WB, Rosell FI, Twitchett MB, Dumont ME, Mauk AG (1998) Biochemistry 37:6124–6131
14. Sinibaldi F, Piro MC, Howes BD, Smulevich G, Ascoli F, Santucci R (2003) Biochemistry 42:7604–7610
15. Sinibaldi F, Howes BD, Piro MC, Caroppi P, Mei G, Ascoli F, Smulevich G, Santucci R (2006) J Biol Inorg Chem 11:52–62
16. Caroppi P, Sinibaldi F, Fiorucci L, Santucci R (2009) Curr Med Chem 16:4058–4065
17. Rytömaa M, Kinnunen PKJ (1994) J Biol Chem 269:1770–1774
18. Rytömaa M, Kinnunen PKJ (1995) J Biol Chem 270:3197–3202
19. Tuominen FK, Wallace CJA, Kinnunen PKJ (2002) J Biol Chem 277:8822–8826
20. Sinibaldi F, Fiorucci L, Patriarca A, Lauceri R, Ferri T, Coletta M, Santucci R (2008) Biochemistry 47:6928–6935
21. Kalanxhi E, Wallace CJA (2007) Biochem J 407:179–187
22. Zou H, Li Y, Liu X, Wang X (1999) J Biol Chem 274:11549–11556
23. Purring-Koch C, McLendon G (2000) Proc Natl Acad Sci USA 97:11928–11931
24. Kagan VE, Tyurin VA, Jiang J, Tyurina YY, Ritov VB, Amoscato AA, Osipov AN, Belikova NA, Kapralov AA, Kini V, Vlasova II, Zhao Q, Zou M, Di P, Svistunenko DA, Kurnikov IV, Borisenko GG (2005) Nat Chem Biol 1:223–232
25. Balakrishnan G, Hu Y, Oyerinde OF, Su J, Groves JT, Spiro TG (2007) J Am Chem Soc 129:504–505
26. Das G, Hickey DR, McLendon D, McLendon G, Sherman F (1989) Proc Natl Acad Sci USA 86:496–499
27. Hope MJ, Nayar R, Mayer LD, Cullis PR (1992) In: Gregoriadis G (ed) Liposome technology, vol 1, 2nd edn. CRC Press, Boca Raton, pp 123–139
28. Pielak GJ, Oikawa K, Mauk AG, Smith M, Kay CM (1986) J Am Chem Soc 108:2724–2727
29. Santucci R, Ascoli F (1997) J Inorg Biochem 68:211–214
30. Pace CN (1975) CRC Crit Rev Biochem 3:1–43
31. Myers JK, Pace CN, Scholtz JM (1995) Protein Sci 4:2138–2148
32. Stellwagen E, Cass R (1974) Biochem Biophys Res Commun 60:371–375
33. Berghuis AM, Brayer GD (1992) J Mol Biol 223:959–976
34. Spaulding LD, Chang CC, Yu N-T, Felton RH (1975) J Am Chem Soc 97:2517–2525
35. Choi S, Spiro TG, Langry KC, Smith KM, Budd DL, La Mar GN (1982) J Am Chem Soc 104:4345–4351
36. Sparks LD, Anderson KK, Medforth CJ, Smith K, Shelnutt JA (1994) Inorg Chem 33:2297–2302
37. Dopner S, Hildebrandt P, Rosell FI, Mauk AG (1998) J Am Chem Soc 120:11246–11255
38. Smulevich G, Bjerrum MJ, Gray HB, Spiro TG (1994) Inorg Chem 33:4629–4634
39. Jordan T, Eads JC, Spiro TG (1995) Protein Sci 4:716–728
40. Indiani C, De Sanctis G, Neri F, Santos H, Smulevich G, Coletta M (2000) Biochemistry 39:8234–8242
41. Zheng J, Ye S, Lu T, Cotton TM, Chumanov G (2000) Biopolymers 57:77–84

42. Caroppi P, Sinibaldi F, Santoni E, Howes BD, Fiorucci L, Ferri T, Ascoli F, Smulevich G, Santucci R (2004) J Biol Inorg Chem 9:997–1006
43. Sinibaldi F, Mei G, Polticelli M, Piro MC, Howes BD, Smulevich G, Santucci R, Ascoli F, Fiorucci L (2005) Protein Sci 14:1049–1058
44. Santoni E, Scatragli S, Sinibaldi F, Fiorucci L, Santucci R, Smulevich G (2004) J Inorg Biochem 98:1067–1077
45. Oellerich S, Wackerbarth H, Hildebrandt P (2002) J Phys Chem B 106:6566–6580
46. Vik SB, Georgevich G, Capaldi RA (1981) Proc Natl Acad Sci USA 78:1456–1460
47. Kapetanaki SM, Silkstone G, Husu I, Liebl U, Wilson MT, Vos MH (2009) Biochemistry 48:1613–1619
48. Mugnol KCU, Ando RA, Nagayasu RY, Faljoni-Alario A, Brochsztain S, Santos PS, Nascimento OR, Nantes IL (2008) Biophys J 98:4066–4077
49. Yoshimura T (1998) Arch Biochem Biophys 264:450–461
50. Yeh S-R, Han S, Rousseau DL (1998) Acc Chem Res 31:727–736
51. Oellerich S, Wackerbarth H, Hildebrandt P (2003) Eur Biophys J 32:599–613